We are IntechOpen, the world's leading publisher of Open Access books Built by scientists, for scientists

4,800
Open access books available

122,000
International authors and editors

135M
Downloads

Our authors are among the

154
Countries delivered to

TOP 1%
most cited scientists

12.2%
Contributors from top 500 universities

CLARIVATE ANALYTICS BOOK CITATION INDEX INDEXED

WEB OF SCIENCE™

Selection of our books indexed in the Book Citation Index in Web of Science™ Core Collection (BKCI)

Interested in publishing with us?
Contact book.department@intechopen.com

Numbers displayed above are based on latest data collected.
For more information visit www.intechopen.com

29

Liquid Crystal - Anisotropic Nanoparticles Mixtures

Vlad Popa-Nita[1], Matej Cvetko[2] and Samo Kralj[3]
[1]*Faculty of Physics, University of Bucharest*
[2]*Regional Development Agency Mura, Murska Sobota*
[3]*Faculty of Natural Science and Mathemetics, University of Maribor*
[1]*Romania*
[2,3]*Slovenia*

1. Introduction

Carbon nanotubes (Iijima, 1991) are one of the most interesting new materials which emerges during the last twenty years. They either consist of a single sheet of carbon atoms covalently bonded in hexagonal arrays rolled up into a cylinder with a diameter of about one nanometer (single-walled nanotubes - SWNTs), or are built up of multiple carbon sheets producing rods with diameters ranging from a few to tens or even hundreds of nanometer (multi-walled nanotubes - MWNTs). The aspect ratio of these objects can vary from hundred to many thousands.

Most of CNTs extraordinary properties of potential use in various applications could be realized in relatively well aligned samples. One method of alignment consists in dispersing the CNTs into a nematic phase of a LC (either thermotropic or lyotropic). For recent reviews see e.g., (Lagerwall & Scalia, 2008; Rahman & Lee, 2009; Zakri, 2007; Zhang & Kumar, 2008).

Theoretically, equilibrium orientation of a single elongated particle immersed in a nematic LC phase is rather well explored (Andrienko et al., 2002; 2003; Brochard & de Gennes, 1970; Burylov & Raikher, 1990; 1994; Hung et. al., 2006). Continuum theory predicts alignment of the particle's longer axis along the nematic director $\vec{n}$ for different types of boundary conditions in the strong anchoring limit case (Brochard & de Gennes, 1970; Burylov & Raikher, 1990; 1994). On the contrary, in the weak anchoring limit the particle may orient either along or perpendicular to the nematic director depending on the boundary conditions (Burylov & Raikher, 1990).

The collective behavior of CNTs dispersed in isotropic solvents or in LC is theoretically relatively weakly explored. Due to their structure and behavior, the CNTs can be consider essentially as rigid-rod polymers with a large aspect ratio (Green et. al., 2009). The steric theory for the electrostatic repulsion of long rigid rods has been used to investigate the SWNT phase behavior in their suspensions (Sabba & Thomas, 2004). Calculations have shown that SWNTs in a good solvent is analogous to the classic rigid-rod system if the van der Waals force between CNTs is overcome by strong repulsive interrods potentials. When the solvent is not good, the van der Waals attractive interactions between the rods are still strong and as a result, only extremely dilute solutions of SWNTs are thermodynamically stable and no LC

phases form at room temperature. The liquid crystallinity of CNTs with and without van der Waals interactions has been analyzed by using the density functional theory (Somoza & Sagui, 2001). In the presence of van der Waals interaction, the nematic as well as the columnar phases occur in the temperature-packing fraction phase diagram in a wide range of very high temperatures. In the absence of van der Waals interaction the system is dominated only by steric repulsive interactions. With an increase of packing fraction, the system undergoes an isotropic-nematic phase transition via a biphasic region. The isotropic-nematic packing fraction decreases with the increase of the aspect ratio of CNTs. The phase behavior of rodlike particles with polydisperse length and solvent-mediated attraction and repulsion is described by an extension of the Onsager theory for rigid rods (Green et. al., 2009). The main conclusion of these theoretical models is that to obtain liquid crystal phases of CNTs at room temperature the strong van der Waals interaction between them must be screened out. This requires a good solvent with an ability to disperse CNTs down to the level of individual tube.

In two recent papers (van der Schoot et. al., 2008; Popa-Nita & Kralj, 2010), two of us presented a phenomenological theory for predicting the alignment of CNTs dispersions in thermotropic nematic LC in the two limits of the anchoring of LC molecules at the CNT surface. We combined the Landau-de Gennes free energy for thermotropic ordering of the LC solvent and the Doi free energy for the lyotropic nematic ordering of CNTs caused by excluded-volume interactions between them. We have analyzed the phase ordering of the binary mixture as a function of the volume fraction of CNTs, the strength of the coupling and the temperature.

However, coupling between LC molecules and nanoparticles (NPs) of regular geometry could in some circumstances give rise to disordered structures with pronounced memory effects. Namely, LC orientational ordering is extremely sensitive to perturbations due to its soft character (de Gennes & Prost, 1993). For example, if a LC is quenched from an isotropic into a nematic phase a continuous symmetry breaking takes place (Imry & Ma, 1975; Kralj et al., 2008; Zurek, 1996). In the isotropic phase all directions are equivalent while in the nematic phase a preferred orientation is singled out locally. Because of finite speed of information propagation well separated regions are causally disconnected. For this reason a domain-type in orientational ordering is inevitable formed. A domain pattern is well characterized by a single characteristic domain size ξ_d. In pure LC the domain size grows with time obeying the scaling law $\xi_d \propto t^{\gamma}$, where $\gamma = 0.5$ in a bulk sample (Bradac et al., 2002). The sample gradually evolves into a homogeneously aligned sample in order to reduce relative expensive domain wall penalties. In a liquid crystal- NP mixture, the NPs could act as pinning centers and consequently domain pattern could be stabilized (Kralj et al., 2008). Therefore, in certain conditions NPs could introduce disorder into a system.

In the present paper we study both ordering and disordering phenomena in a LC-NP mixture. In the first part of the present paper we focus on LC induced ordering of CNT. We present comparatively the results of our phenomenological model in the two limiting cases: i) **the weak anchoring limit** where the interaction between CNTs and LC molecules is thought to be sufficiently weak not to cause any director field deformations in the nematic host fluid and ii) **the strong (rigid) anchoring limit** where the CNT causes the nematic director field distortions generating topological singularities. In the second part we study conditions where orientational ordering of a NP-LC mixture could be essentially short ranged.

The plan of the paper is as follows. In Sec. 2 we study LC driven orientational ordering of CNTs. In Subsection 2.1 our phenomenological model is introduced. In Sec. 2.2 we analyze ordering of CNT in the isotropic LC phase. The trictitical behavior is analyzed in

detail in Sec. 2.3. Possibility of homogeneous alignment of CNTs in investigated in Sec. 2.4. Both weak and strong anchoring LC-CNT interactions are taken into account. In Sec. 3 possible disordering effects in LC-NP mixtures are analyzed using a simple lattice-type semimicroscopic description. The semimicroscopic model is described in Sec. 3.1 and the corresponding simulation method in Sec. 3.2. The NPs induced domain type stabilization of LC ordering is demonstrated in Sec. 3.3. In the last section we summarize our conclusions.

2. LC induced CNT ordering

We first discuss conditions under which LC orientational ordering could be used in order to align immersed anisotropic NPs. We confine our interest to CNTs due to their importance in various applications. The ordering of LC-CNT mixtures is treated using a mean field type phenomenological model.

2.1 Free energy

The free energy per unit volume of the CNTs-LC binary mixture consists of four contributions

$$f = f_{mix} + f_{CNT} + f_{LC} + f_C. \tag{1}$$

The first term in Eq. (1) is the free energy density of isotropic mixing of CNTs and LC that in the framework of Flory lattice theory is given by (Flory, 1953)

$$f_{mix}/k_BT = v_{CNT}^{-1}\Phi \ln \Phi + v_{LC}^{-1}(1-\Phi)\ln(1-\Phi) + v_0^{-1}\chi\Phi(1-\Phi), \tag{2}$$

where k_B is the Boltzmann constant, T is the absolute temperature, Φ is the volume fraction of CNT, $1-\Phi$ is the volume fraction of LC, and $\chi \equiv U_0/k_BT$ is the Flory-Huggins interaction parameter related to the isotropic interaction between CNT and LC (Flory, 1953). In the following, we assume $\chi > 0$ (positive free energy of mixing), this being the most usual case, at least when van der Waals interactions are dominant. Here $v_{CNT} \approx \frac{\pi}{4}LD^2$ approximates volume occupied by a carbon nanotube of length L and diameter D. The volume of a LC molecule of length l and diameter d is given by $v_{LC} \approx \frac{\pi}{4}ld^2$. In the following we consider that the volume of a LC molecule is equal to the volume of a cell in the Flory lattice (Flory, 1953) ($v_{LC} = v_0$). The first two terms in Eq. (2) represent the entropy of isotropic mixing of LC and CNT components neglecting their orientational degree of ordering.

The free energy density representative of the excluded volume effects responsible for the first order nematic-isotropic transition of CNT is expressed as (Doi & Edwards, 1989)

$$f_{CNT}/k_BT = \frac{\Phi}{v_{CNT}}\left[\frac{1}{2}\left(1-\frac{u}{3}\right)S_{CNT}^2 - \frac{u}{9}S_{CNT}^3 + \frac{u}{6}S_{CNT}^4\right]. \tag{3}$$

The parameter u is related to the volume fraction of CNT by the relation $u = \Phi L/D$. The model neglects the van der Waals attractions between CNTs which are responsible for their tendency to form bundles. The degree of orientational ordering of CNT is given by the order parameter S_{CNT}. Perfectly aligned CNT correspond to $S_{CNT} = 1$, and isotropic ordering is signaled by $S_{CNT} = 0$. On increasing Φ this term enforces the first order orientational phase transition of CNT from the isotropic phase of CNT with $S_{CNT} = 0$, to the nematic phase of CNT phase with $S_{CNT} = (1+\sqrt{9-24/u})/4$. The first order nematic-isotropic phase transition takes place at $u = u_{NI} = 27/10$ and $S_{CNT}(u_{NI}) = 1/3$. The limits of stability of nematic and isotropic phases are given by $u^+ = 8/3$ ($S_{CNT}^+ = 1/4$) and $u^* = 3$ ($S_{CNT}^* = 1/2$).

For the thermotropic uniaxial nematic LC component we use the standard Landau-de Gennes (de Gennes & Prost, 1993) free energy density in terms of the nematic order parameter S_{LC}

$$f_{LC} = (1-\Phi)\left[\frac{3}{2}a(T-T^*)S_{LC}^2 - \frac{3}{4}BS_{LC}^3 + \frac{9}{4}CS_{LC}^4\right], \tag{4}$$

where $(1-\Phi)$ accounts for the part of the volume not taken up by LC. The quantities T^* (the undercooling limit temperature of the isotropic phase of the pure liquid crystal), a, B, and C are material-dependent constants. This free energy density enforces the weakly first order phase transition from the isotropic phase to the nematic phase of LC. At $T = T_{NI} = T^* + B^2/(24aC)$, the two phases of LC, nematic ($S_{nem\,0} = B/6C$) and isotropic ($S_{iso} = 0$) coexist in equilibrium. The detailed derivation of the coupling free energy density term f_C in the two limiting regimes has been presented previously (van der Schoot et. al., 2008; Popa-Nita & Kralj, 2010). Here we give only the final expressions. The two regimes can be defined by the relation between the radius of the particle R and the surface extrapolation length $d_e = K/W$, where K is the Frank elastic constant and W is the anchoring energy.

i) **the weak anchoring limit** ($R << d_e$)- the anchoring is not able to produce large deformations in the surrounding nematic matrix. In this limit the coupling free energy density writes as (van der Schoot et. al., 2008)

$$f_C = -\gamma_w\Phi(1-\Phi)S_{LC}S_{CNT}\left(1-\frac{1}{2}S_{CNT}\right), \tag{5}$$

where the coupling constant is given by $\gamma_w = 4W/6R$. Depending on the value of R and considering a typical value of anchoring energy of 10^{-6}N/m, the coupling constant of the weak anchoring regime can range between $10^{-3} - 10^3$N/m^2.

ii) **strong anchoring limit** ($R >> d_e$) - the anchoring is rigid and gives rise to topological singularities of the nematic director which cause strong interaction between the dispersed nanotubes. In this limit the coupling free energy density writes as (Popa-Nita & Kralj, 2010)

$$f_C = -\gamma_s\Phi(1-\Phi)S_{LC}^2S_{CNT}\left(1-\frac{1}{2}S_{CNT}\right), \tag{6}$$

where the coupling constant is given by $\gamma_s = 2K/3R^2$. Depending on the value of R and considering a typical value of elastic constant of 10^{-11}N the coupling constant of the strong anchoring regime can range between $10^3 - 10^7$N/m^2.

Using Eqs. (2), (3), (4), (5), and (6), the total phenomenological free energy density in the weak anchoring limit becomes:

$$\begin{aligned} f = {} & k_BT\left[v_{CNT}^{-1}\Phi\ln\Phi + v_{LC}^{-1}(1-\Phi)\ln(1-\Phi) + v_{LC}^{-1}\chi\Phi(1-\Phi)\right] \\ & + \frac{k_BT\Phi}{v_{CNT}}\left[\frac{1}{2}\left(1-\frac{u}{3}\right)S_{CNT}^2 - \frac{u}{9}S_{CNT}^3 + \frac{u}{6}S_{CNT}^4\right] \\ & + (1-\Phi)\left[\frac{3}{2}a(T-T^*)S_{LC}^2 - \frac{3}{4}BS_{LC}^3 + \frac{9}{4}CS_{LC}^4\right] \\ & - \gamma_w\Phi(1-\Phi)S_{LC}S_{CNT}\left(1-\frac{1}{2}S_{CNT}\right), \end{aligned} \tag{7}$$

while in the strong anchoring limit, only the last term differ:

$$
\begin{aligned}
f = k_B T \left[v_{CNT}^{-1} \Phi \ln \Phi + v_{LC}^{-1} (1-\Phi) \ln(1-\Phi) + v_{LC}^{-1} \chi \Phi (1-\Phi) \right] \\
+ \frac{k_B T \Phi}{v_{CNT}} \left[\frac{1}{2} \left(1 - \frac{u}{3} \right) S_{CNT}^2 - \frac{u}{9} S_{CNT}^3 + \frac{u}{6} S_{CNT}^4 \right] \\
+ (1-\Phi) \left[\frac{3}{2} a (T - T^*) S_{LC}^2 - \frac{3}{4} B S_{LC}^3 + \frac{9}{4} C S_{LC}^4 \right] \\
- \gamma_s \Phi (1-\Phi) S_{LC}^2 S_{CNT} \left(1 - \frac{1}{2} S_{CNT} \right).
\end{aligned} \tag{8}
$$

In calculations we consider a regime determined by the following geometrical and material parameters. We limit to CNT of characteristic dimensions $L \approx 400$ nm and $R \approx 1$ nm. For LC molecules we set $L \approx 3$ nm and $R \approx 0.25$ nm, corresponding to a typical nematogen. For LC material constants we chose as representative pentylcyanobiphenyl (5CB) LC, for which $T^* = 306$ K, $a \approx 3.5 \cdot 10^4$ J $\cdot$ m$^{-3} \cdot$ K^{-1}, $B \approx 7.1 \cdot 10^5$ J $\cdot$ m^{-3}, $C \approx 4.3 \cdot 10^5$ J $\cdot$ m^{-3}, $K \sim 10^{-11}$ N (Oswald & Pieranski, 2005). This choice yields $S_{nem\,0} \approx 0.28$ and $T_{NI} = T^* + B^2/24aC \approx 307.5$ K.

Using this phenomenological form of the free energy, in the following sections we present the phase behavior of the binary mixture of CNTs and LC as a function of temperature, volume fraction and the coupling strength.

2.2 Dispersion of CNTs in the isotropic phase of LC

In this case, $S_{LC} = 0$, the coupling free energy densities (5) and (6) cancel and the free energy density becomes

$$
\begin{aligned}
f/k_B T = v_{CNT}^{-1} \Phi \ln \Phi + v_{LC}^{-1} (1-\Phi) \ln(1-\Phi) + v_{LC}^{-1} \chi \Phi (1-\Phi) \\
+ \frac{\Phi}{v_{CNT}} \left[\frac{1}{2} \left(1 - \frac{u}{3} \right) S_{CNT}^2 - \frac{u}{9} S_{CNT}^3 + \frac{u}{6} S_{CNT}^4 \right].
\end{aligned} \tag{9}
$$

The equilibrium between the isotropic ($S_{CNT} = 0$) and the nematic phase ($S_{CNT} > 0$) of CNTs is determined by equating the chemical potentials of CNTs ($\mu_{CNT} = v_{CNT}[f + (1 - \phi)\partial f/\partial\phi]$) and LC ($\mu_{LC} = v_{LC}(f - \phi \partial f/\partial\phi)$) in the two phases. The value of S_{CNT} is obtained by minimizing the free energy with respect to S_{CNT}.

In the absence of the isotropic interaction term ($\chi = 0$), for our set of geometric parameters the nematic-isotropic coexistence is determined by the following values of parameters: ($\Phi_{iso} = 0.013487$, $S_{CNT} = 0$) and ($\Phi_{nem} = 0.013513$, $S_{CNT} = 0.3365$) and correspondingly the relative variation of volume fraction of CNTs at the transition (the Flory chimney) is about 0.19%. The phase gap in this condition is very narrow indeed less than the 1% predicted by Onsager and Flory for monodisperse lyotropic LC. On the basis of the polarized light microscopy, Song and Windle (Song & Windle, 2005) have estimated a biphasic range between 1% and 4% in an aqueous dispersion of MWNTS. This comparatively large range of the biphasic region is plausibly caused by the polidispersity in terms of length, diameter, and straightness of the nanotubes as well as the possibility of segregation of the more nematogenic tubes.

In Figure 1, we have plotted the relative variation of the volume fraction of the CNTs at the nematic-isotropic phase transition as a function of the isotropic interaction parameter χ.

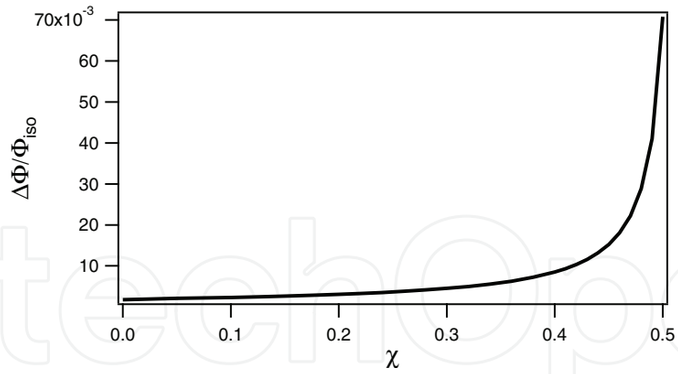

Fig. 1. The relative variation of the volume fraction of CNTs at the nematic-isotropic phase transition in the isotropic phase of LC.

Because the isotropic interaction parameter is proportional with reciprocal temperature (here we did not consider this dependence), the volume fraction gap at the transition increases with lowering the temperature; the poor solvent for CNTs becomes poorer lowering the temperature. For values of χ larger than ≈ 0.4 the relative variation of the volume fraction at the transition increases considerably with the value of χ. The predicted value of $\Delta\Phi/\Phi_{iso} = 1\%$ is obtained for $\chi = 0.42$.

2.3 Tricritical point

The free energy density is given now by the general forms (7) and (8), respectively.
For very small values of the coupling parameter γ_w (or equivalently γ_s), the nematic-isotropic phase transition of the CNTs is first order and the order parameter jumps at the transition from zero to some non-zero value depending on the value of the coupling parameter. With increasing the interaction parameter, the transition becomes continuous at a tricritical value $\gamma_{w,t}$ (or equivalently $\gamma_{s,t}$). The tricritical point where the discontinuous phase transition becomes continuous is obtained by solving the equations $\partial^2 f/\partial S_{LC}^2 = \partial^3 f/\partial S_{LC}^3 = 0$. They yield at the tricritical point universal values for the order parameter $S_{CNT}^{(t)} = 1/6$ and volume fraction $\Phi_t = 0.01296$. The tricritical values of the coupling parameter γ_t as a function of temperature are presented in Figure 2.
With decreasing the temperature, as S_{LC} increases, the external field felt by the CNTs increases and the nematic-isotropic phase transition of CNTs becomes continuous for increasingly lower values of interaction parameter. Our estimates of the coupling constant suggest that for typical value of parameters, $\gamma >> \gamma_t$ for both limiting cases, meaning that in the nematic phase of LC, the nematic-isotropic phase transition of CNTs becomes a continuous transition.
To illustrate how in the limit of low values of coupling parameter the isotropic-nematic phase transition of the CNTs is affected by the nematic host fluid, the phase diagram of the coexisting volume fractions as a function of the coupling parameter is plotted in Figure 3 for both limiting regimes. The binodals are drawn at the undercooling limit temperature of the isotropic phase ($T^* = 307.56K$).
In both limiting regimes, the gaps of the volume fractions decrease with increasing the coupling constant and becomes zero for $\gamma_w = \gamma_{w,t} = 79.6$ N/m^2 (for weak anchoring) and for $\gamma_s = \gamma_{s,t} = 191$ N/m^2 for strong anchoring case, respectively. The isotropic-nematic phase transition of CNTs takes place at lower volume fraction with increasing the coupling constant.

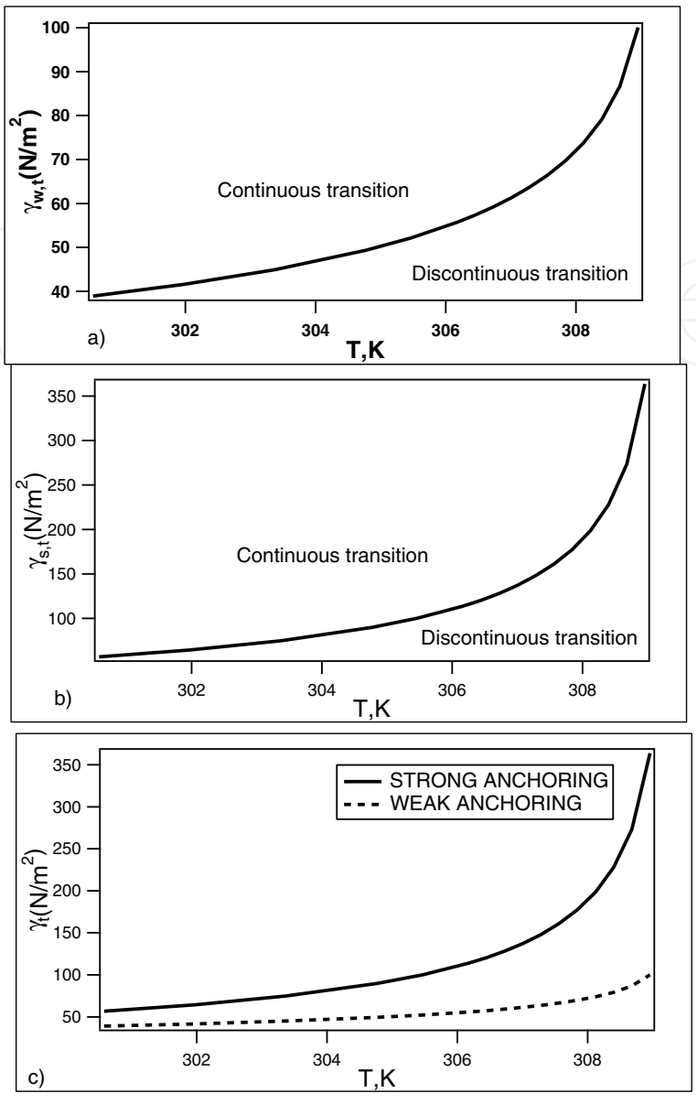

Fig. 2. The tricritical values of the coupling parameter γ_t as function of temperature. The weak anchoring limit case is represented in Fig. 2a. In Fig. 2b is shown the strong anchoring limit case, while in Fig. 2c the both regimes are represented.

2.4 Homogeneous mixture

One of the most challenging task for realizing the applications in optoelectronics is to homogeneously disperse the CNTs into the nematic host, as CNTs have a tendency to aggregate into networks and fibrils (MWNTs) within the dispersion due to the van der Waals interactions between the nanotubes. The three different standard approaches to obtain the homogeneous dispersion are reviewed in (Lagerwall & Scalia, 2008; Rahman & Lee, 2009).

To calculate the phase diagram of a homogeneous mixture, we use the free energy density given by Eq. (7) (for the weak anchoring case) and the same quantity given by Eq. (8) (corresponding to the strong anchoring case) with a constant volume fraction Φ of the CNTs. The equilibrium values of the order parameters S_{CNT} and S_{LC} are obtained by minimizing

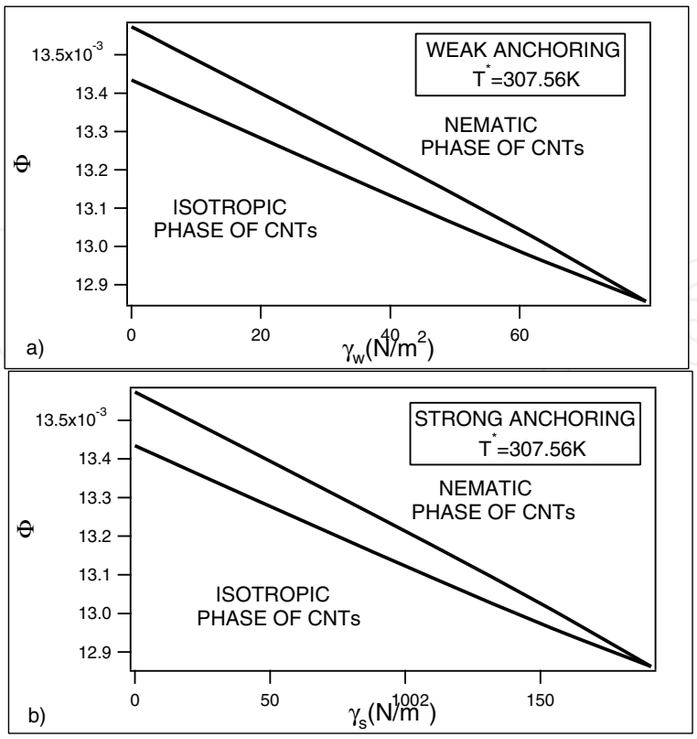

Fig. 3. Phase diagram of CNTs in the nematic host fluid. Indicated are the coexisting volume fractions in the isotropic and nematic phases discussed in the main text. The weak anchoring case is shown in Fig. 3a, while Fig. 3b presents the strong anchoring case.

the free energy density ($\partial f/\partial S_{CNT} = \partial f/\partial S_{LC} = 0$). The corresponding phase diagrams are plotted and discussed in the next two sections.

2.4.1 Weak anchoring case

The phase diagram (Φ, T) in the weak anchoring regime for a typical value of the coupling constant $\gamma = 6.6 \cdot 10^5$ N/m^2 is plotted in Fig. 4.

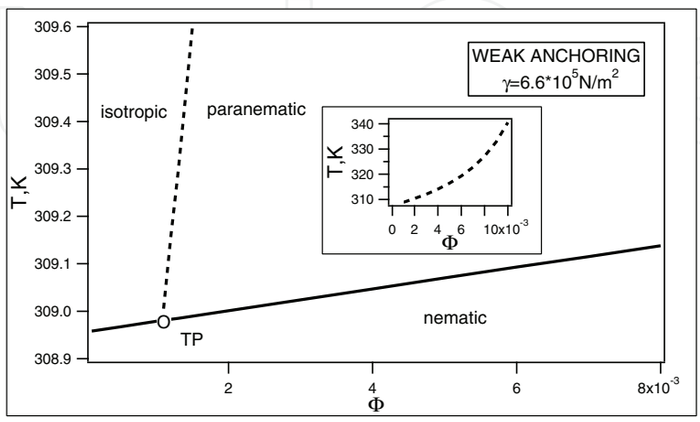

Fig. 4. The (Φ, T) phase diagram of a homogeneous mixture in the weak anchoring limiting case.

Three different regions are to be distinguished. **The isotropic region** corresponds to a total absence of the orientational order (both components are in the isotropic phase), **the paranematic region** is characterized by a very small degree of the orientational order of both components, while in **the nematic region** both components possess a relatively large degree of orientational order. The dashed line defines a second order (the order parameter is continuous at the transition, while its derivative with respect to temperature has a jump) isotropic-paranematic phase transition (inside the figure we have shown this line for larger values of the temperature). The first segment ($\Phi \leq 0.00108$) of the continuous line corresponds to first order (the order parameter has a jump at the transition) nematic-isotropic phase transition of both components. The second segment ($\Phi \geq 0.00108$) corresponds to the first order nematic-paranematic phase transition of the both components. The circle defines the triple point of the system that has the coordinates $\Phi_t = 0.00108$ and $T = 308.98$ K. The increase of nematic-isotropic phase transition temperature (shown by the continuous line in Fig. 4) is experimentally verifiably (Duran et. al., 2005; Lebovka et. al., 2008) and could be explained by the fact that CNTs act as heterogeneous nucleation agents for LC.
To see in more detail the characteristics of these phase transitions we have plotted in Figure 5 the order parameters profiles as a function of volume fraction of CNTs for two different values of the temperature.

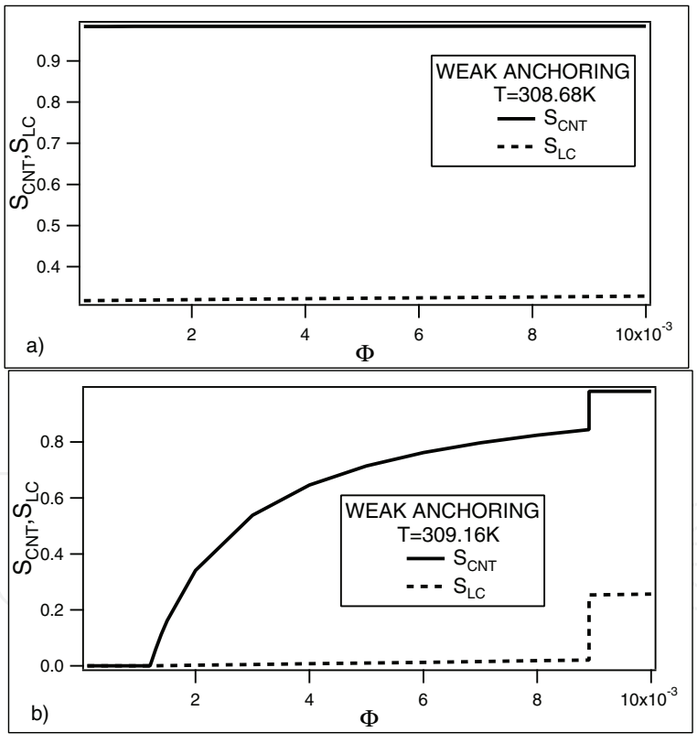

Fig. 5. The order parameters profiles of CNTs (continuous line) and LC (dotted line) for $\gamma = 6.6 \cdot 10^5$ N/m^2 and for two different values of the temperature.

In Figure 5a, the order parameters profiles are shown for $T = 308.68$ K, value that belongs to the nematic region in Fig. 4. There is no phase transition for this value of temperature and as consequence the order parameters are continuous and CNTs are almost perfectly aligned ($S_{CNT} \approx 1$) for all values of volume fraction (see the continuous line). On the

contrary, the value of temperature in Figure 5b ($T = 309.16$ K) corresponds to a second order isotropic-paranematic phase transition at a small value of the volume fraction and to a first order paranematic-nematic phase transition at a larger value of the volume fraction. In this case, the CNTs are strongly aligned at relatively large value of the volume fraction.
In Figure 6, we have shown the order parameters profiles as a function of temperature for two different values of the volume fraction of CNTs.

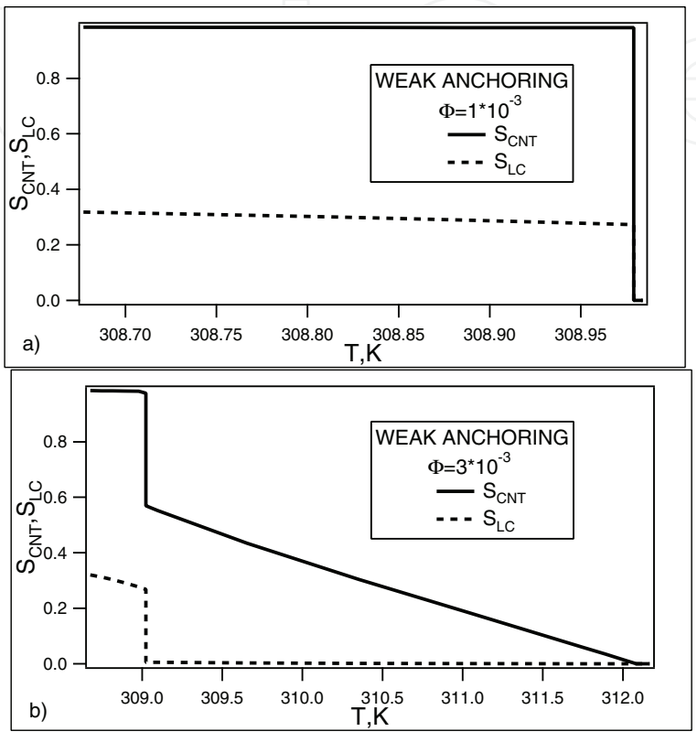

Fig. 6. The order parameters profiles of CNTs (continuous line) and LC (dotted line) for $\gamma = 6.6 \cdot 10^5$ N/m^2 and two different values of the volume fraction.

In Figure 6a, the order parameter profiles are shown for a small value of the volume fraction ($\Phi = 1 \cdot 10^{-3}$). For this value of the volume fraction, increasing the temperature the only transition is the first order nematic-isotropic phase transition (see Figure 4) during which both order parameters jump to zero. The larger value of the volume fraction of Figure 6b induces two phase transitions (see Figure 4): a first order nematic-paranematic phase transition at a lower value of the temperature during which both order parameters jump at lower values and a second order paranematic-isotropic phase transition at a larger value of the temperature during which both order parameters decrease continuously to zero.

2.4.2 Strong anchoring case

The corresponding phase diagram (Φ, T) for a typical value of the coupling constant $\gamma = 6.6 \cdot 10^5$ N/m^2 is plotted in Fig. 7. Even if the corresponding phase diagram is similar to the weak anchoring limiting case, there are some differences which we discuss in the following.
Also in this strong anchoring case, there are three different regions in the phase diagram. **The region I** corresponds to a total absence of the orientational order (both components are in the isotropic phase), **region II** corresponds to a nematic phase of CNT and an isotropic phase of

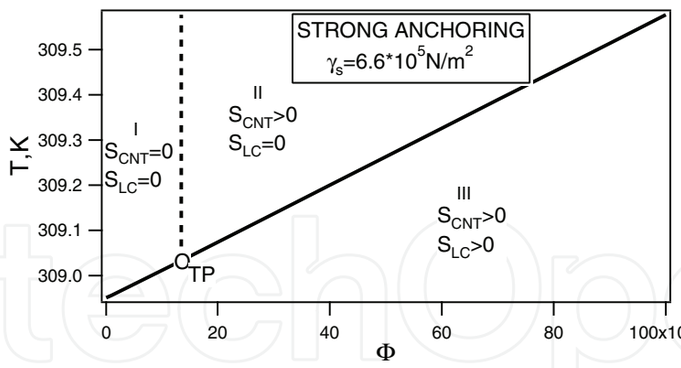

Fig. 7. The (Φ, T) phase diagram of a homogeneous mixture in the strong anchoring limiting case.

LC, while in **the region III** both components are in the nematic phase. The vertical dashed line defines a second order isotropic (region I)-nematic (region II) phase transition of the CNTs in the isotropic phase of LC. The first segment ($\Phi \leq 0.0135$) of the oblique continuous line corresponds to the first order isotropic-nematic phase transition of CNTs as well as to the first order isotropic-nematic phase transition of LC. The second segment ($\Phi \geq 0.0135$) corresponds to the first order isotropic-nematic phase transition of the LC and to a first order nematic-nematic phase transition of the CNTs (in the region II the degree of orientational order of CNTs is lower that that of region III and in passing from region II to region III there is a jump of the CNTs order parameter). The circle defines the triple point of the system that has the coordinates $\Phi_t = 0.0135, T = 309.03$ K. The experimental fact (Duran et. al., 2005; Lebovka et. al., 2008) that the isotropic-nematic phase transition temperature of LC increases with the volume fraction of CNTs is again theoretically explained by the present model.
In Figure 8 the order parameters profiles as a function of volume fraction of CNTs for two different values of the temperature are shown.
The value of the temperature ($T = 309$ K) in Figure 8a, corresponds to one isotropic-nematic first order phase transition obtained increasing the volume fraction (transition between regions I and III in Figure 7), phase transition during which both order parameters jump from zero to finite values. CNTs becomes almost perfectly aligned at very small values of the volume fractions. The value of temperature in Figure 8b ($T = 309.2$ K) induces a second order isotropic-nematic phase transition of CNTs at a relatively small volume fraction (transition between regions I and II in Figure 7) followed by a first order isotropic-nematic phase transition of both components LC (transition between regions II and III in Figure 7). In this case, the CNTs are strongly aligned at relatively large value of the volume fraction.
The order parameters profiles as a function of temperature for two different values of the volume fraction of CNTs are plotted in Figure 9.
In Figure 9a, the order parameter profiles are shown for a small value of the volume fraction ($\Phi = 1 \cdot 10^{-2}$). For this value of the volume fraction, increasing the temperature, the transition is the first order nematic-isotropic phase transition (transition between regions III and I in Figure 7) during which both order parameters jump to zero. The larger value of the volume fraction of Figure 9b induces a first order phase transition of both components (transition between regions III and II in Figure 7). The order parameter jump of CNTs is very small (in both region III and II, CNTs are in nematic phase but with different degree of orientational order), while the order parameter of LC jumps from a finite value to zero.

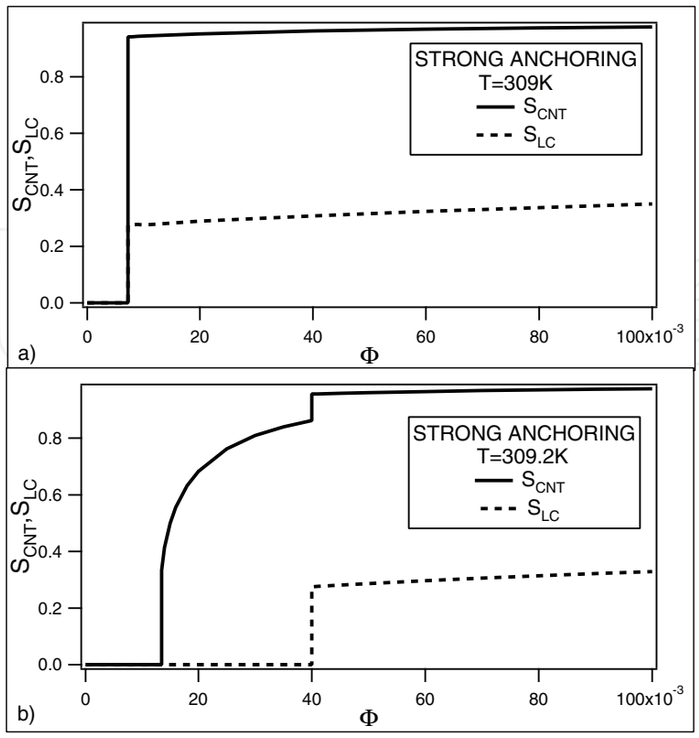

Fig. 8. The order parameters profiles of CNTs (continuous line) and LC (dotted line) for $\gamma = 6.6 \cdot 10^5$ N/m^2 and two different values of the temperature.

3. Nanoparticle induced disorder

We next consider mixtures of LC molecules and anisotropic NPs. It is of interest to find conditions for which NPs could impose relatively strong disorder to surrounding LC molecules. In order to find simple possible key conditions for such phenomena we constrain our investigations to appropriate type of interactions among NPs and LC molecules. We set LC molecules and NPs to be of comparable size. We do not impose any inherent disorder to systems. Molecules of both types are assumed to have regular shape and interaction potential which are intuitively expected to enforce order on a macroscopic scale. Below we demonstrate that symmetry breaking and NP driven stabilization of LC domains could destroy LC long range order in case of appropriate initial conditions.

3.1 Interaction energy

We confine our interest to mixtures of liquid crystals and anisotropic nanoparticles, where both components have comparable characteristic geometrical length. We assume that concentrations of NPs are relatively low. In order to study structural properties of the ensembles we use a lattice-spin type model (Bellini et al., 2000; Lebwohl & Lasher, 1972) in three dimensional space. The lattice points form a three dimensional cubic lattice characterized by the lattice constant a_0. The number of sites equals N^3, where we typically set $N = 80$. The NPs are randomly distributed within the lattice with probability p. For $p = 1$ all the sites are occupied by NPs and a pure LC sample is obtained in the limit $p = 0$. Therefore, value of p is equal to the volume fraction Φ of NPs.

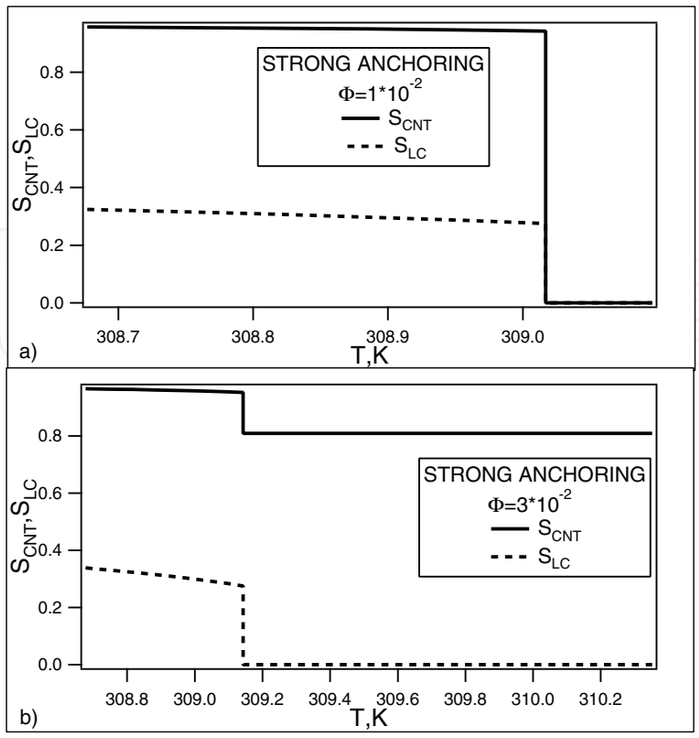

Fig. 9. The order parameters profiles of CNTs (continuous line) and LC (dotted line) for $\gamma = 6.6 \cdot 10^5$ N/m^2 and two different values of the temperature.

A key anisotropic property of a LC molecule or a nanoparticle at a site $\overrightarrow{r}_i$ is roughly represented by the unit vector $\overrightarrow{n}_i$ and $\overrightarrow{m}_i$, respectively. We assume the head-to-tail invariance of LC molecules. Therefore, the orientations $\pm\overrightarrow{n}_i$ are equivalent due to a rod-like character of molecules. In the continuum limit $\overrightarrow{n}_i$ roughly corresponds to the nematic director field. On the other hand sign of $\overrightarrow{m}_i$ matters. For example, such property of a NP could be due to its magnetic or electric dipole. We henceforth refer to $\overrightarrow{n}_i$ ($\overrightarrow{m}_i$) as the nematic (magnetic) spin. The interaction energy E of the system is given by (Cvetko et al., 2009; Krasna et al., 2010; Lebwohl & Lasher, 1972)

$$E = -\sum_i \sum_j J_{ij}^{(n)} \left(\overrightarrow{n}_i \cdot \overrightarrow{n}_j\right)^2 - \sum_i \sum_j J_{ij}^{(m)} \left(\overrightarrow{m}_i \cdot \overrightarrow{m}_j\right) + \sum_i \sum_j J_{ij}^{(nm)} \left(\overrightarrow{n}_i \cdot \overrightarrow{m}_j\right)^2. \quad (10)$$

The constants $J_{ij}^{(n)}$, $J_{ij}^{(m)}$, and $J_{ij}^{(nm)}$ stand for the coupling strengths LC-LC, NP-NP, and LC-NP, respectively. The sums run over all the sites and only the interactions between first neighbors are different from zero. The first term describes interaction among LC molecules, where $J_{ij}^{(n)} = J > 0$ for neighboring molecules. Therefore, a pair of LC molecules tend to orient either parallel or antiparallel. The coupling between neighboring NPs is determined with $J_{ij}^{(m)} = J_{NP} > 0$, enforcing antiparallel orientation. On the contrary, neighboring LC-NP pairs tend to be aligned perpendicularly due to $J_{ij}^{(nm)} = w > 0$. The latter condition is crucial in order to introduce strong disorder into the system and related memory effects. Note that replacing

the 2nd term by Lebwohl-Lasher type coupling $-\sum\sum J_{ij}^{(m)}\left(\vec{m}_i \cdot \vec{m}_j\right)^2$ would not introduce qualitatively different behavior.
In the subsequent work distances are scaled with respect to a_0. The interaction energies are measured with respect to J, i.e. we set $J = 1$.

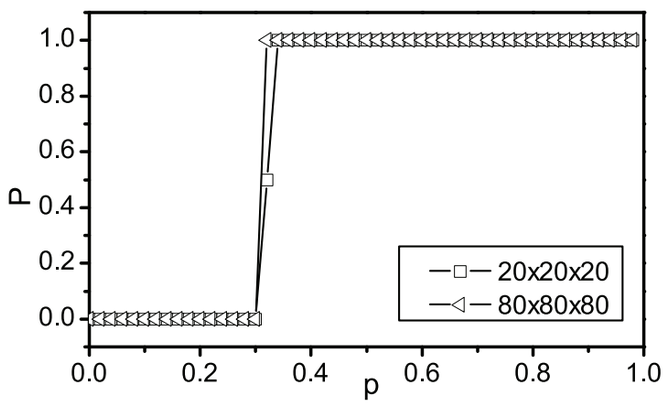

Fig. 10. The percolation probability P as a function of p and system size. For a finite value of N the percolation threshold p_c is defined as $P(p_c) = 0.5$. We obtain $p_c \sim 0.3$.

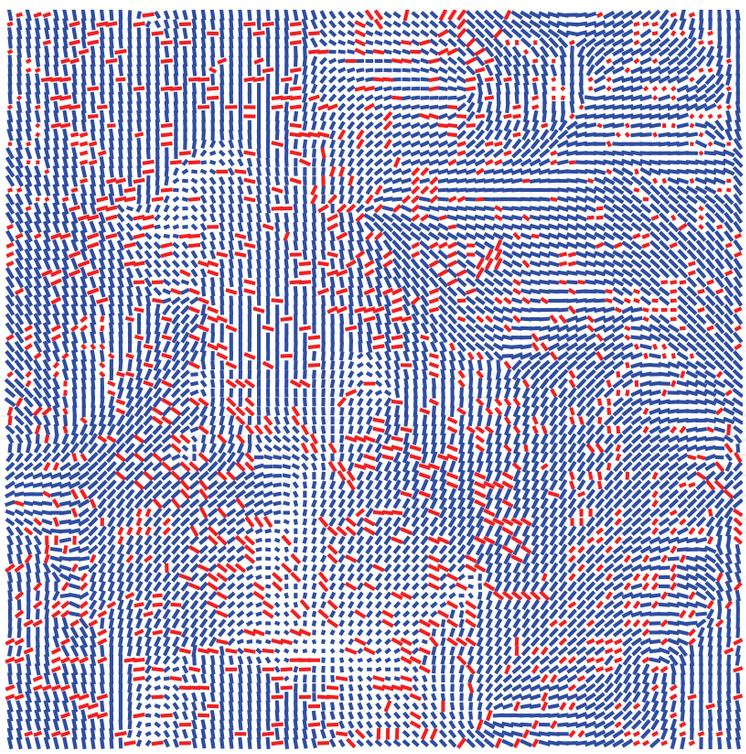

Fig. 11. Representative cross-sections of a LC+NP mixture. NPs and LC molecules are colored with red and blue, respectively. $p = 0.2$.

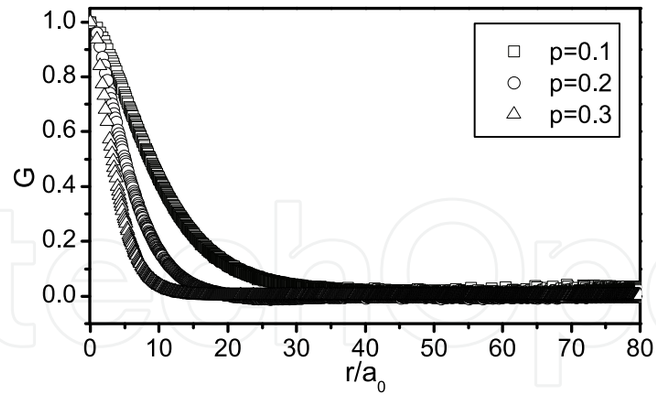

Fig. 12. Typical $G(r)$ plots for different concentrations of NPs.

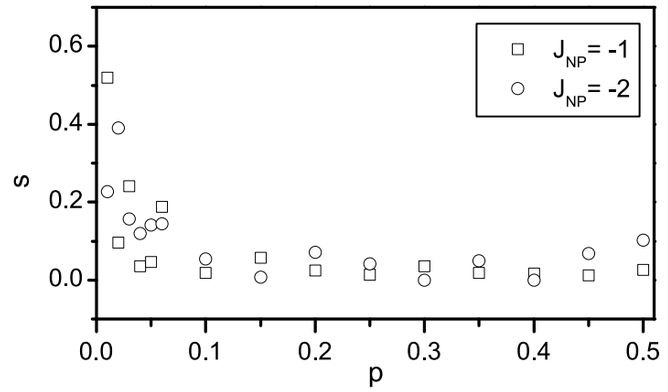

Fig. 13. Characteristic $s(p)$ behavior. The random field regime extends roughly between $p = p_{RF} \sim 0.1$ and $p \sim p_c \sim 0.3$.

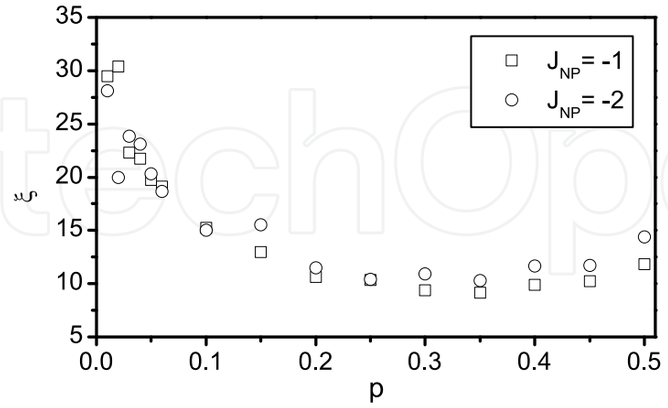

Fig. 14. The correlation length ξ as a function of p.

3.2 Simulation method and measured quantities

All simulations take place at zero temperature where we minimize the interaction energy given by Eq.(10) with respect to orientation of nematic and magnetic spins. The corresponding

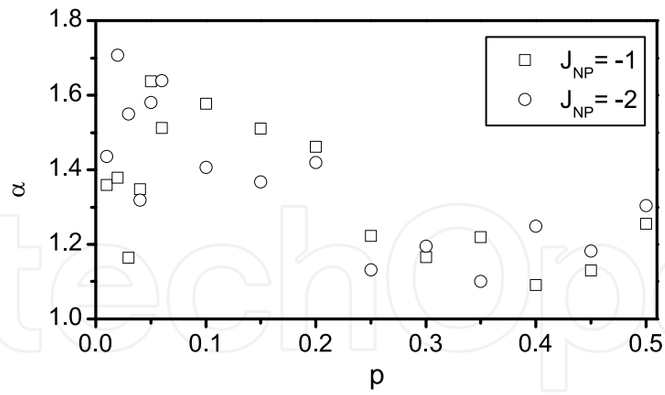

Fig. 15. The coefficient α as a function of p.

set of equations have been solved using the Newton's method. Periodic boundary conditions are imposed. Simulations are carried over different values of p, J_{NP} and w. The concentration regime from $p = 0$ to $p > p_c$ is investigated where p_c stands for the percolation threshold of NPs.

Both nematic and NP spins are initially randomly orientationally distributed. Experimentally such conditions correspond to quenches from high temperature isotropic phase states. Maximum simulation box sizes are set to $N = 80$. In order to diminish the influence of statistical variations ten simulations starting from statistically different initial configurations have been carried out for a given set of parameters.

In simulations we calculate steady state configurations. For obtained steady state configuration we calculate the orientational correlation function G of LC molecules. It measures the orientational correlation of LC spins as a function of their mutual separation r and is defined as (Cvetko et al., 2009)

$$G(r) = \frac{1}{2}\left\langle 3\left(\overrightarrow{n}_i \cdot \overrightarrow{n}_j\right)^2 - 1\right\rangle. \tag{11}$$

The brackets denote the average over all lattice sites that are separated by a distance r. Our test simulations indicate that $G(r)$ does not depend on orientation of $\overrightarrow{r}$, therefore we focus on r dependence. The $G(r)$ properties are as follows. For completely correlated nematic spins aligned along a single symmetry breaking orientation it holds $G(r) = 1$. On the contrary $G(r) = 0$ signals completely uncorrelated nematic spins. Because each spin is necessarily parallel with itself it holds $G(0) = 1$. Furthermore, we normally expect the correlation function to be a decreasing function of distance r. If a long range LC order exists in the system then $G(r \to \infty) = S^2 > 0$, where S stands for the nematic orientational order parameter. On the contrary, short range order (SRO) or quasi long range order (QLRO) are signaled by $G(r \to \infty) = 0$.

To obtain structural details from the simulation results we fit $G(r)$ to an empirical ansatz Eq.((Cvetko et al., 2009)).

$$G(r) = (1 - s)e^{-(r/\xi)^{\alpha}} + s. \tag{12}$$

Here the coherence length ξ, the stretched exponential parameter α, and s are adjustable parameters. The coherence length ξ measures distance over which nematic spins are relatively

strongly correlated. The stretched exponential parameter α is introduced by analogy with the stretched exponential temporal decay which occurs in many glassy systems. The parameter s directly reflects the range of ordering. Namely, $s = 0$ for SRO (Cvetko et al., 2009).

3.3 Nanoparticle stabilized domain patterns

We study domain pattern stabilization as a function of p and typical interaction strengths. Qualitative changes in the behavior are expected below and above the percolation threshold of NPs. For this reason we first analyze the percolation characteristics in our systems. For a given concentration p of NPs we calculate the probability P that there exists a connected path of NPs between the oppositely placed boundaries of a simulation cell. The $P(p)$ plot in Figure 10 reveals that on increasing p the percolation threshold is reached at $p_c \sim 0.3$. In the thermodynamic limit the dependence displays a phase transition type of behavior, where P plays the role of order parameter. For a finite simulation cell a pretransitional tail appears below p_c, and at the transition steepness of $P(p)$ increases with increasing N. In simulations we use large enough values of N so that finite size effects are negligible.

The presence of NPs enforces to LC molecules a certain amount of disorder. If the latter is strong enough LC long range could be destroyed. A typical LC-NP pattern is shown in Fig. 11 where short range order is evident. The range of ordering can be inferred from $G(r)$. In Figure 12 we plot typical correlation functions for different values of p. The calculated $G(r)$ dependencies are fitted with the ansatz Eq.(12).

In the regime $p < p_c$ the network of NPs is not percolated. Due to frustrating tendencies (i.e. the LC-LC interaction favors parallel or antiparallel alignment, while the LC-NP interaction enforces perpendicularly oriented configurations) it is anticipated that in this regime disorder strength is apparent. This is clearly shown in the $s(p)$ plot in Fig. 13. We observe $s(p) \sim 0$ in appropriate interval of concentrations, roughly between $p \sim p_{rf} \sim 0.1$ and $p \sim p_c$ (for $w \sim J_{NP}$. Note that on increasing p above the percolation threshold the $s(p)$ dependence begins to increases with p. For concentrations, where $s(p) \sim 0$, the system exhibits short range order (at least approximatively). Therefore, the disorder is strong enough to destroy long range nematic LC ordering. We refer to the concentration range $p_{rf} < p < p_c$ as the **random field regime.**

We next study structural behavior across the percolation threshold. Characteristic structural properties are shown in Fig. 14 and 15. As expected a qualitative change in behavior is observed on crossing the percolation thresholds, which is particularly evident from the $\xi(p)$ plots (Fig. 14). We see that above the percolation threshold $\xi(p)$ tends to increase. The reason for this is formation of correlated order in NPs orientational order. Consequently, the LC component also becomes ordered. One sees increase in s in the regime $p > p_c$. The changes in α are shown in Fig. 15. We see that in the **random field regime** $\alpha(p)$ values relatively strongly fluctuate. On approaching the percolation threshold values of α tend to assemble closer to $\alpha = 1$, which would be reached in absence of disorder.

4. Conclusions

In the first part of the present paper, using a mean field type phenomenological model, we have examined the phase and structural behavior of a binary mixture composed of CNTs dispersed in thermotropic LC in two anchoring regimes. In the weak anchoring limit of the nematic LC molecules at the nanotube's surface, the CNTs alignment is caused by the anisotropic interfacial tension of the nanotubes in the nematic host fluid. In this

case, the interaction between CNTs and LC molecules is sufficiently weak to not cause any director deformations in the nematic and the coupling parameter is given by $\gamma_w = 4W/6R$ (independent of L). In the strong anchoring limit, the nematic ordering around nanotube is distorted (this case includes two different situations, either the nematic director is nonsingular or topological defects are present). Now, the coupling parameter is given by $\gamma_s = 2K/3R^2$.
First, we have considered the dispersion of CNTs in the isotropic phase of LC (in this case $S_{LC} = 0$ and the interaction free energy densities given by Eqs. (5) and (6) cancel. By fitting the relative variation of the volume fraction of CNTs $(\Phi_{nem} - \Phi_{iso})/\Phi_{iso}$ at the transition with the experimental value, we have obtained the value of Flory-Huggins interaction parameter $\chi = 0.42$.
Second, in both anchoring cases, the first-order nematic - isotropic phase transition of CNTs dispersed in the nematic phase transforms into a continuous transition for a strong enough coupling to the nematic host fluid. The corresponding tricritical value of the coupling parameter increases with increasing temperature being larger in the strong anchoring limit case (see Figure 2). The numerical estimate of the coupling constants in the two anchoring regimes indicates that the coupling is so strong that CNTs are far above the tricritical point, meaning that the nematic-isotropic phase transition is a continuous one.
Third, in both anchoring cases, we have plotted the phase diagram of the homogeneous mixture for the same value of the coupling parameter. In both cases, three regions of the phase diagram could be distinguished and correspondingly the existence of triple points are shown. We mention that in both anchoring cases, the nematic-isotropic phase transition temperature of LC increases with the volume fraction of CNTs, a well-known experimental result.
It is to be stressed that the model presented does not consider two important features of the system: the van der Waals interaction between CNTs and the polydispersity of CNTs. In the future work we intend to include this features into the model.
In the second part of the paper we have shown that in a LC-NP mixture frozen domain type structure of orientational order might appear, yielding (at least approximate) short range orientational ordering. In order to find out key ingredients giving rise to such phenomena we use a semimicroscopic lattice model. The essential ingredients of the model are simple and regular. Pure systems of LC molecules (i.e. $\Phi = p = 0$) or NPs ($p = 1$) tend to form regular structures. We assume that phase separation is absent and that NPs are essentially homogeneously distributed within a liquid crystal phase. If the LC-NP coupling tends to orient molecules perpendicularly (or close to such configuration), the resulting configurations might be trapped in domain type structures exhibiting short range order. The main reason for this is softness of the LC component and consequently relatively strong susceptibility to various perturbations in orientational ordering. We considered concentration ranges between $p = 0$ and slightly above the percolation threshold p_c. In case of comparable sizes of LC molecules and NPs we obtained $p_c \sim 0.3$. If a mixture was quenched from an isotropic phase, than structures exhibiting essentially short range order were obtained in the concentration range between $p \sim 0.1$ and $p \sim p_c$. Below $p \sim 0.1$ NPs are too diluted to destroy LC long range order. On the other for $p > p_c$ the NPs become percolated and consequently at least partially orientationally ordered. This order is transferred also to the LC component. Therefore, within the interval $p \sim 0.1$ and $p \sim p_c$ mixtures could display glass like states with pronounced memory effects. In our future study we plan to investigate in detail glassy characteristics and memory effects within this interval.

5. Acknowledgments

V.P.-N. is very grateful to P. Poulin and P. van der Schoot for very helpful discussions. Matej Cvetko acknowledges support of the EU European Social Fund. Operation is performed within the Operative program for development of human resources for the period 2007-2013.

6. References

Andrienko D., Allen M. P., Skacej G., and Žumer S. (2002) Defect structures and torque on an elongated colloidal particle immersed an a liquid crystal host. *Phys. Rev. E* Vol. 65, 041702, 7 pp.

Andrienko D., Tasinkevych M., Patricio P., Allen M. P., and Telo da Gamma M. M. (2003) Forces between eleongated particles in a nematic colloid. *Phys. Rev. E* Vol. 68, 051702, 5pp.

Bellini T., Buscagli M., Chiccoli C., Mantegazza F., Pasini P., and Zannoni C. (2000) Nematics with quenched disorder: What is left when long range order is disrupted?, Phys. Rev. Lett. *Small* Vol 85, No 5, pp.1008-11.

Bradac Z., Kralj S., and Zumer S., (2002) Molecular dynamics study of isotropic-nematic quench, Phys.Rev.E *Small* 65, 021705-1-10.

Brochard F. and de Gennes P. G. (1970) Theory of magnetic suspensions in liquid crystals. *J. Phys. (Paris)* Tome 31, pp. 691-699 .

Burylov S. V. and Raikher Yu. L. (1990) On the orientation of an anisometric particle suspended in a bulk uniform nematic. *Phys. Lett. A* Vol. 149, number 5,6, pp. 279-283.

Burylov S. V. and Raikher Yu. L. (1994) Orientation of a solid particle embedded in a monodomain nematic liquid crystal. *Phys. Rev. E* Vol. 50, Number 1, pp 358-367.

Cvetko M., Ambrozci M. and Kralj S. (2009) Memory effects in randomly perturbed systems exhibiting continuous symmetry breaking, Liq. Cryst. *Small* Vol 36, No. 1, pp. 33-41.

Doi M. and Edwards S. F. (1989), *Theory of Polymer Dynamics* Clarendon, Oxford.

Duran H., Gazdecki B., Yamashita A., Kyu T.(2005) Effect of carbon nanotubes on phase transitions of nematic liquid crystals. *Liq. Cryst.*, Vol. 32, No. 7, pp. 815-821.

Flory P. J. (1953) *Principles of Polymer Chemistry* Cornell University Press, Ithaca.

de Gennes P. G. Prost J. (1993) *The Physics of Liquid Crystals* Oxford University Press, Oxford.

Green M. J., Behabtu N., Pasquali M., Adams W. W. (2009) Nanotubes as polymers. *Polymer*, Vol. 50, pp. 4979-4997.

Green M. J., Parra-Vasquez A. N. G., Behabtu N., Pasquali M. (2009) Modeling the phase behavior of polydisperse rigid rods with attractive interactions with applications to single-walled carbon nanotubes in superacids. *J. Chem. Phys.*, Vol. 131, 084901, 10 pp.

Hung F. R., Guzman O., Gettelfinger T., Abbott N. L., and de Pablo J. J. (2006) Anisotropic nanoparticles immersed in a nematic liquid crystal: Defect structures and potantial of mean force. *Phys. Rev. E* Vol. 74, 011711, 12 pp.

Iijima S. (1991), Helical microtubules of graphitic carbon. *Nature*, Vol 354, pp. 56-58.

Imry Y. and Ma S. (1975) Random-filed instability of ordered state of continuous symmetry, Phys. Rev. Lett. *Small* Vol 35, No. 21, pp. 1399-1401.

Kralj S., Bradac Z., and Popa-Nita V., (2008) The influence of nanoparticles on the phase and structural ordering for nematic liquid crystals, J. Phys.: Condens. Matter *Small* Vol 20, pp. 244112-244122 .

Krasna M., Cvetko M., and Ambrozic M., (2010) Symmetry breaking and structure of a mixture of nematic liquid crystals and anisotropic nanoparticles, Bel. J. Org. Chem. *Small* Vol 6, Article No. 74.

Lagerwall J. P. F. and Scalia G (2008) Carbon nanotubes in liquid crystals. *J. Mater. Chem.* Vol. 18, pp. 2890-2898.

Lebovka N., Dadakove T., Lysetskiy L., Melezhyk O., Puchkovska G., Gavrilko T., Baran J., Drodz M. (2008) Phase transitions, intermolecular interactions and electrical conductivity in carbon multiwalled nanotubes/nematic liquid crystal composites. *J. Molecular Structure* Vol. 887, pp. 135-143.

Lebwohl P. A., Lasher G. (1972) Nematic-Liqid-Crystal Order - Monte Carlo calculation, Phys. Rev. A *Small* Vol 6, No. 1, pp. 426

Oswald P. and Pieranski P. (2005), *Nematic and Cholesteric Liquid crystals; concepts and physical properties illustrated by experiments* Taylor and Francis Group, CRC Press, in Liquid Crystals Book Series, Boca Raton.

van der Schoot P., Popa-Nita V., and Kralj S. (2008) Alignment of Carbon Nanotubes in Nematic Liquid Crystals. *J. Phys. Chem. B* Vol. 112, pp. 4512-4518.

Rahman M. and Lee W. (2009) Scientific duo of carbon nanotubes and nematic liquid crystals. *J. Phys. D: Appl. Phys.* Vol. 42, 063001, 12 pp.

Sabba Y. and Thomas E. L. (2004) High-Concentration Dispersion of Single-Wall Carbon Nanotubes. *Macromolecules* Vol. 37, pp. 4815-4820.

Somoza A. M., Sagui C., and Roland C. (2001) Liquid-crystal of capped carbon nanotubes. *Phys. Rev. B* Vol. 63, 081403 4 pp.

Song W. and Windle A. H. (2005) Isotropic-Nematic Phase Transition of Dispersion of Multiwall Carbon Nanotubes. *Macromolecules* Vol. 38, pp. 6181-6188.

Popa-Nita V., and Kralj S. (2010) Liquid crystal-carbon nanotubes mixtures. *J. Chem. Phys.* Vol. 132, 024902, 8 pp.

Zakri C. (2007) Carbon nanotubes and liquid crystalline phases. *Liquid Crystals Today*, Vol. 16, No. 1, pp 1-11.

Zhang S. and Kumar S. (2008) Carbon Nanotubes as Liquid Crystals. *Small* Vol. 4, No. 9, pp. 1270-1283.

Zurek W. (1996) Cosmological experiments in condensed matter systems, Phys. Rep. *Small* Vol 276, No. 4, pp. 177-221.

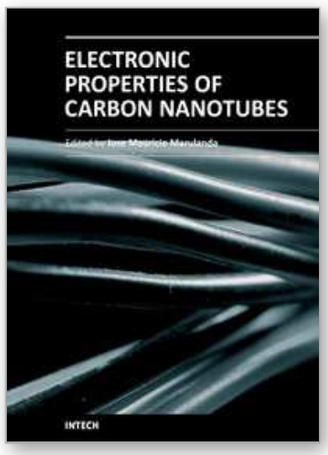

Electronic Properties of Carbon Nanotubes

Edited by Prof. Jose Mauricio Marulanda

ISBN 978-953-307-499-3
Hard cover, 680 pages
Publisher InTech
Published online 27, July, 2011
Published in print edition July, 2011

Carbon nanotubes (CNTs), discovered in 1991, have been a subject of intensive research for a wide range of applications. These one-dimensional (1D) graphene sheets rolled into a tubular form have been the target of many researchers around the world. This book concentrates on the semiconductor physics of carbon nanotubes, it brings unique insight into the phenomena encountered in the electronic structure when operating with carbon nanotubes. This book also presents to reader useful information on the fabrication and applications of these outstanding materials. The main objective of this book is to give in-depth understanding of the physics and electronic structure of carbon nanotubes. Readers of this book should have a strong background on physical electronics and semiconductor device physics. This book first discusses fabrication techniques followed by an analysis on the physical properties of carbon nanotubes, including density of states and electronic structures. Ultimately, the book pursues a significant amount of work in the industry applications of carbon nanotubes.

INTECH
open science | open minds

InTech Europe
University Campus STeP Ri
Slavka Krautzeka 83/A
51000 Rijeka, Croatia
Phone: +385 (51) 770 447
Fax: +385 (51) 686 166
www.intechopen.com

InTech China
Unit 405, Office Block, Hotel Equatorial Shanghai
No.65, Yan An Road (West), Shanghai, 200040, China
中国上海市延安西路65号上海国际贵都大饭店办公楼405单元
Phone: +86-21-62489820
Fax: +86-21-62489821

IntechOpen